NAVAL POSTGRADUATE SCHOOL

MONTEREY, CALIFORNIA

THESIS

INNER SHELF WIND AND WAVE STRESS BALANCE: MODEL SENSITIVITY ANALYSIS ASSOCIATED WITH WAVE SHOALING

by

Christie Underwood

December 2020

Thesis Advisor: James H. MacMahan
Second Reader: Edward B. Thornton

THIS PAGE INTENTIONALLY LEFT BLANK

REPORT DOCUMENTATION PAGE	*Form Approved OMB No. 0704-0188*

1. AGENCY USE ONLY *(Leave blank)*	**2. REPORT DATE** December 2020	**3. REPORT TYPE AND DATES COVERED** Master's thesis

4. TITLE AND SUBTITLE
INNER SHELF WIND AND WAVE STRESS BALANCE: MODEL SENSITIVITY ANALYSIS ASSOCIATED WITH WAVE SHOALING

5. FUNDING NUMBERS

6. AUTHOR(S) Christie Underwood

7. PERFORMING ORGANIZATION NAME(S) AND ADDRESS(ES)
Naval Postgraduate School
Monterey, CA 93943-5000

8. PERFORMING ORGANIZATION REPORT NUMBER

9. SPONSORING / MONITORING AGENCY NAME(S) AND ADDRESS(ES)
N/A

10. SPONSORING / MONITORING AGENCY REPORT NUMBER

11. SUPPLEMENTARY NOTES The views expressed in this thesis are those of the author and do not reflect the official policy or position of the Department of Defense or the U.S. Government.

12a. DISTRIBUTION / AVAILABILITY STATEMENT
Approved for public release. Distribution is unlimited.

12b. DISTRIBUTION CODE
A

13. ABSTRACT (maximum 200 words)

New open-ocean formulations that define the total wind stress (τ_{total}) at the air-sea boundary that include contributions from both wind (τ_{wind}) and waves (τ_{wave}) were evaluated across the wave shoaling region of the inner shelf. Traditional τ_{total} open ocean formulations have underestimated measured τ_{total} across the inner shelf. The new formulations spectrally account for the "swell" wave contributions and have been modified to account for the depth (h) dependence of wave shoaling. Swell is defined when phase speed, c_p, is greater than $1.14U_{10}$, wind speed. The difference between the h-independent, deep-water c_p, to the h-dependent c_p occurs for U_{10}, <12 m s^{-1} and h<20m. This defines the parameter space for which swell provides additional contributions across the inner shelf, where the remainder should be described by traditional open-ocean formulations. As c_p decreases with decreasing h, swell contribution relative to U_{10} decreases with decreasing h. Shoaling wave heights result in a 50% higher shallow-water swell τ_{wave} compared to deep water, and vary as a function of wave height for U_{10}, <6 m s^{-1}. Constraining τ_{wave} by a weighted probability density function of Monterey Bay climatology, τ_{wave} is larger than τ_{wind} for U_{10}, <6m s^{-1}. τ_{wave} increases variability with decreasing U_{10}. In summary, the conditions that define τ_{wave} for the inner shelf are sensitive to wave shoaling, are limited by U_{10} , and, though limited, produce the largest τ_{wave} in shallow water.

14. SUBJECT TERMS
air-sea interaction, inner shelf, momentum flux, wave boundary layer, wind stress, wave stress, shoaling

15. NUMBER OF PAGES
61

16. PRICE CODE

17. SECURITY CLASSIFICATION OF REPORT	**18. SECURITY CLASSIFICATION OF THIS PAGE**	**19. SECURITY CLASSIFICATION OF ABSTRACT**	**20. LIMITATION OF ABSTRACT**
Unclassified	Unclassified	Unclassified	UU

NSN 7540-01-280-5500

Standard Form 298 (Rev. 2-89)
Prescribed by ANSI Std. 239-18

THIS PAGE INTENTIONALLY LEFT BLANK

Approved for public release. Distribution is unlimited.

INNER SHELF WIND AND WAVE STRESS BALANCE: MODEL SENSITIVITY ANALYSIS ASSOCIATED WITH WAVE SHOALING

Christie Underwood
Lieutenant Commander, Royal Australian Navy
BS, University of New South Wales (UNSW@ADFA) Australia, 2007
GDS, Bureau of Meteorology Australia, 2012
MA, University of New South Wales (UNSW@ADFA) Australia, 2014

Submitted in partial fulfillment of the
requirements for the degree of

MASTER OF SCIENCE IN PHYSICAL OCEANOGRAPHY

from the

NAVAL POSTGRADUATE SCHOOL
December 2020

Approved by: James H. MacMahan
Advisor

Edward B. Thornton
Second Reader

Peter C. Chu
Chair, Department of Oceanography

THIS PAGE INTENTIONALLY LEFT BLANK

ABSTRACT

New open-ocean formulations that define the total wind stress (τ_{total}) at the air-sea boundary that include contributions from both wind (τ_{wind}) and waves (τ_{wave}) were evaluated across the wave shoaling region of the inner shelf. Traditional τ_{total} open ocean formulations have underestimated measured τ_{total} across the inner shelf. The new formulations spectrally account for the "swell" wave contributions and have been modified to account for the depth (h) dependence of wave shoaling. Swell is defined when phase speed, c_p, is greater than $1.14U_{10}$, wind speed. The difference between the h-independent, deep-water c_p, to the h-dependent c_p occurs for U_{10}, <12 m s^{-1} and h<20m. This defines the parameter space for which swell provides additional contributions across the inner shelf, where the remainder should be described by traditional open-ocean formulations. As c_p decreases with decreasing h, swell contribution relative to U_{10} decreases with decreasing h. Shoaling wave heights result in a 50% higher shallow-water swell τ_{wave} compared to deep water, and vary as a function of wave height for U_{10}, <6 m s^{-1}. Constraining τ_{wave} by a weighted probability density function of Monterey Bay climatology, τ_{wave} is larger than τ_{wind} for U_{10}, <6m s^{-1}. τ_{wave} increases variability with decreasing U_{10}. In summary, the conditions that define τ_{wave} for the inner shelf are sensitive to wave shoaling, are limited by U_{10} , and, though limited,produce the largest τ_{wave} in shallow water.

THIS PAGE INTENTIONALLY LEFT BLANK

TABLE OF CONTENTS

THIS PAGE INTENTIONALLY LEFT BLANK

LIST OF FIGURES

LIST OF ACRONYMS AND ABBREVIATIONS

H15	Högström et al. (2015) model
MABL	marine atmospheric boundary layer
MB	Monterey Bay
MOST	Monin-Obukhov Similarity Theory
NDBC	National Data Buoy Center
S09	Semedo et al. (2009) model
TKE	turbulent kinetic energy
WBL	wave boundary layer

THIS PAGE INTENTIONALLY LEFT BLANK

I. INTRODUCTION

The atmosphere and ocean are coupled by exchanges that occur at the air-ocean interface determined by properties of the boundary layers on either side of the water surface (Jones and Toba 2001). Tangential stress (τ) is expressed as the vertical flux of horizontal momentum quantified as a drag force per unit area (Jones and Toba 2001). The stress facilitates wind-wave development, air-ocean mixing and ocean current transport (Dawe and Thompson 2006; Klein and Coste 1984; Munk and Wunsch 1998). In the following analysis, it is assumed the vector wind stress is only in the *x*-direction of the mean wind, given by:

$$\tau = -\rho_{atm}\overline{u'w'} \tag{1.1}$$

where ρ_{atm} is the atmospheric density, $(\overline{u'w'})$ is the time averaged product of the horizontal and vertical perturbation components (momentum flux), where $\overline{v'w'} = 0$. The negative sign of the momentum flux denotes a downward direction (-*z*) indicating that the wind stress is transferred from the atmosphere to ocean (Garratt 1992). The total stress (τ_{total}) at the air-sea boundary is a sum of contributions from wind induced shear stress (τ_{wind}) and wave induced stress (τ_{wave}) as follows:

$$\tau_{total} = \tau_{wind} + \tau_{wave} \tag{1.2}$$

where viscous stress scales are too small to affect changes in the mean flow (~1 mm of the surface layer) and are assumed negligible to be included in (1.2) (Chen et al. 2019; Hanley and Belcher 2008; Kaimal and Finnigan 1994; Wyngaard and LeMone 1980).

In general, open-ocean formulations ignore τ_{wave}. The wave effects are incorporated in τ_{wind} in Eq (1.2) through the aerodynamic roughness length (z_0) in the well-known logarithmic (i.e., "law of the wall") profile based on Monin-Obukhov Similarity Theory (MOST) defined by:

$$\bar{u}(z) = \frac{u_*}{\kappa} \ln\left(\frac{z}{z_0}\right) \tag{1.3}$$

where $\bar{u}$ is the mean wind speed as a function of vertical elevation z, κ is the von Karman constant, and u_* is the magnitude of the kinematic surface stress referred to as the frictional velocity (Stull 1988). u_* is defined as:

$$u_* = \sqrt{\left|\frac{\tau}{\rho_{atm}}\right|} = \sqrt{\left|\overline{(u'w')}\right|}. \tag{1.4}$$

τ_{total} is re-written in terms of u_* as follows:

$$\tau_{total} = \rho_{atm} u_*^2. \tag{1.5}$$

Note, since τ_{total} is a vector, the sign of u_* needs to be accounted for when $u_* < 0$.

z_0 is related to the geometric roughness of the sea surface and, for the ocean, defines the height of the wave boundary layer (WBL) where fluctuations produced by waves are no longer felt (Chalikov and Babanin 2019). Above z_0 for two-dimensional stationary flow, no horizontal gradients, and constant shear stress in the turbulent boundary layer, MOST applies and wind speed decreases exponentially with decreasing height as per the log wind profile, Eq (1.3). The most common estimate for z_0 is the Charnock (1955) estimate:

$$z_0 = 0.012 \frac{u_*^2}{g} \tag{1.6}$$

where 0.012 is the empirically estimated Charnock constant that accounts for the ocean wave roughness. Kitaigorodskii and Volkov (1965) first determined that z_0 is related to wave phase speed c_p. When the wind speed is faster (slower) than c_p, the roughness is enhanced (reduced) (Drennan et al. 2003; Harris 1966; Kitaigorodskii and Volkov 1965).

The ratio of the relative speed is referred to as wave age described as $\frac{c_p}{U_{10}}$ or $\frac{c_p}{u_*}$ (Drennan et al. 2005; Drennan et al. 2003). The parameterization of z_0 has evolved based on wave age as follows (Drennan et al. 2005; Kitaigorodskii and Volkov 1965):

$$\frac{z_0 g}{u_*^2} = f\left(\frac{c_p}{u_*}\right). \tag{1.7}$$

A fundamental aspect of Eq. (1.7) is that wave age is based on the bulk average of wave statistics, where c_p is estimated by the peak wave period using the deep-water relationship (Donelan et al. 1993; Drennan et al. 2003).

The ocean-atmospheric community typically describe the inherent ocean wave effects with the dimensionless, parameterized, drag coefficient $\left(C_D\right)$ which is analogous to z_0. C_D is commonly used because it more directly relates the mean wind, U_{10} to τ_{total}:

$$\tau_{total} = \rho_{atm} C_D U_{10}^2. \tag{1.8}$$

The relationship between C_D and z_0 is obtained by re-writing Eq (1.8) for C_D using Eq (1.5):

$$C_D = \frac{u_*^2}{U_z^2} \tag{1.9}$$

followed by substituting Eq (1.9) into Eq (1.3) resulting in:

$$C_D = \left(\kappa \ln\left(\frac{z_0}{z}\right)\right)^2 \tag{1.10}$$

(Ortiz-Suslow et al. 2015; Shabani et al. 2014).

Most C_D observations and corresponding parameterizations occurred for the open ocean (Shabani et al. 2014), which are independent of water depth. How C_D observations and parameterization varies by depth for the inner-shelf and surfzone is the focus herein.

For the open ocean, predictions of C_D are valid for certain wind ranges (~4-20 m s^{-1}) in deep-water, where the seas are fully developed (Garratt 1977; Large and Pond 1980). For the inner-shelf (defined from 2–30 m) and near a coastal inlet, Ortiz-Suslow et al. (2015) found C_D values were an O(2.5) higher than the open ocean. Within the wave breaking surf zone region, MacMahan (2017) and Shabani et al. (2014) found O(2) higher stresses than the open ocean. This suggests that open-ocean parameterizations are unlikely to accurately predict C_D over the inner-shelf region. This was confirmed by Ortiz-Suslow et al. (2018) by comparing stress measurements from the inner-shelf region to seven bulk C_D parameterization models, which consistently underestimated the observed drag by a factor of 2–4.

It is hypothesized that underestimates of C_D across the inner shelf are firstly related to the wave dependence on water depth, which increases with decreases in water depth. Secondly, it is suggested that better estimates would be achieved by accounting for the wave contributions by computing the net wave contributions spectrally for sea and swell vice average wave statistics used in z_0 models. These considerations have been recognized in differing aspects, as described next.

Semedo et al. (2009) (S09) developed an analytical model based on a near-surface jet that occurs during swell conditions observed by Hanley and Belcher (2008). The S09 spectrally describes Eq. (1.2) and will be discussed below. Chen et al. (2019) adapted this model for the inner shelf accounting for depth dependence and compared the model to unique tower observations acquired in 16 m water depth. The S09 has two tuning coefficients that Chen et al. (2019) modified with their observations. Högström et al. (2015) (H15) developed an empirical model based on bulk statistics derived from spectral wave observations accounting for sea and swell. H15 validated their model with existing observations in deep water (Högström et al. 2015). Ortiz-Suslow et al. (2018) modified the

H15 for depth dependence and compared it with a few small boat observations. H15 predictions were within ~30% accuracy, with the model-observation comparisons reported to be substantially improved when depth effects were considered (Ortiz-Suslow et al. 2018).

Since S09 was analytically derived it can provide vertical profile estimates, whereas H15 is limited to one elevation at 10 m. More observations are required to establish clarity on the spatial evolution of the dynamics across the shoaling region due to the limitations of one tower at one depth from Chen et al. (2019) and only a few case studies from Ortiz-Suslow et al. (2018). Owing to the limited exisiting observations, a sensitivty of the S09 and H15 models are explored further herein. To our knowledge, these are the only two relatively simple models that account for sea swell waves seperately and allow for further exploration and refinement.

The inner shelf is synonymous with the shoaling region and decreasing water depths from offshore to onshore. Here, wave speeds decrease while wave heights increase, with decreasing depths. The phase speed, c_p, is dependent on the wave period (or frequency) and the water depth. Ocean waves exist across a board band of frequencies and c_p correspondingly varies across frequency per water depth. The low frequency spectral range is considered swell (decay) that propagates faster than U_{10} and the high frequency spectral range is considered sea (growth) that propagates slower than U_{10}. The S09 and H15 models define the frequency cut-off $\left(n_p\right)$ to be when wave forcing transitions from growth to decay. n_p is related to when $U_{10} = 1.14c_p$. H15 and S09 use the deep water relationship for c_p, described as:

$$c_0 = \frac{gT}{2\pi} \tag{1.11}$$

where *T* is the wave period and *g* is the acceleration due to gravity (9.81 m s^{-1}). Eq. (1.11) excludes the influence of *h* (Dean and Dalrymple 1991). Ortiz-Suslow et al. (2018) recognizes, and Chen et al. (2019) uses the general c_p relationship that accounts for *h*:

$$c_p = \frac{g}{\omega}\tanh(kh) \tag{1.12}$$

where ω is the angular frequency (rad s^{-1}), k is the wavenumber (rad m^{-1}). Chen et al. (2019) used the peak frequency for Eq. 1.12 and then solved for the transition frequency based on U_{10}, which is not accurate. The transition frequency is dependent only on h and U_{10}, and can be solved directly by re-writing Eq. (1.12) for n_p:

$$n_p = \frac{g\tanh(kh)}{1.14U_{10}(2\pi)} \tag{1.13}$$

The wave surface elevation spectra for swell and sea are given by:

$$H_{rms}^{swell} = 2\sqrt{2}\sqrt{\int_0^{n_p} S(n)\,dn} \tag{1.14}$$

$$H_{rms}^{sea} = 2\sqrt{2}\sqrt{\int_{n_p}^{\infty} S(n)dn} \tag{1.15}$$

where significant wave height $H_{sig} = \sqrt{2}H_{rms}$. Note, the S09 model uses H_{rms} and H15 uses H_{sig}. All wave heights will be described as H_{rms} but will be adjusted for H15 model.

The anticipated effects on the vertical wind profile and stress balance at the sea surface transitioning from offshore to the inner shelf in the shoaling wave region is illustrated in Figure 1. The offshore zone represents conditions observed by Chen et al. (2019) where waves propagate faster than the mean wind (old, swell) and perform work on the atmosphere above. This leads to an upward $\overline{u'w'}$, a reduction in surface stress, and a wind maximum near the surface and a WBL at ~30 m. c_p decreases across the inner shelf giving rise to conditions that are conducive to a reversal of $\overline{u'w'}$ direction from positive (z) to negative ($-z$) relative to the prevailing mean winds, increasing surface stress. The impact to stress at the surface is reflected in the magnitude of u_*.

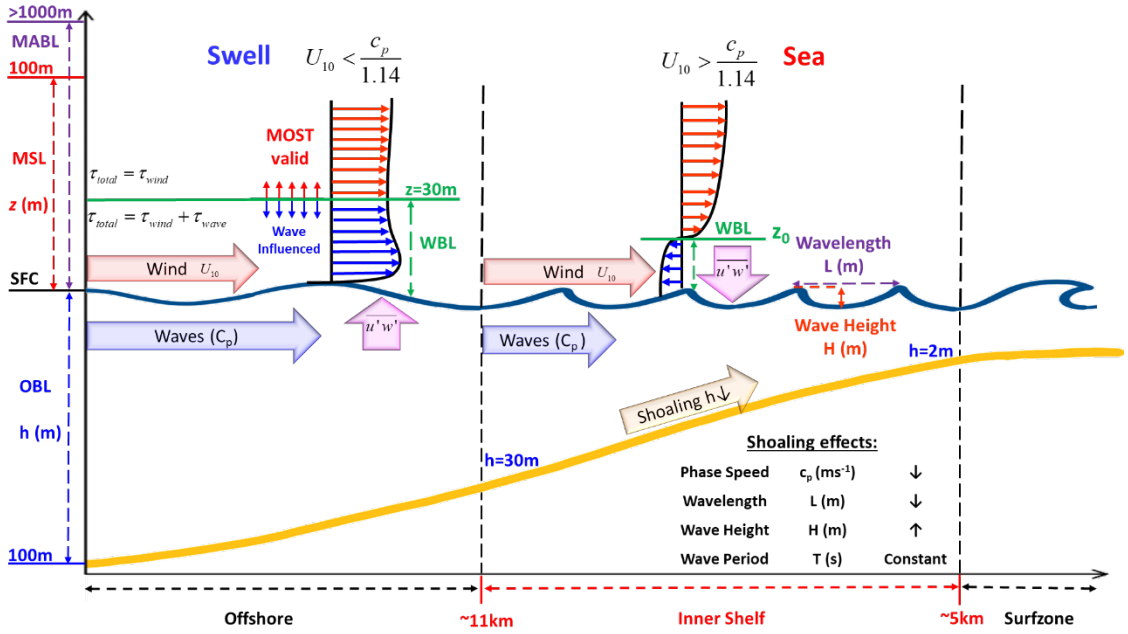

Figure 1. Shoaling effects and anticipated $\overline{u'w'}$ direction in the inner shelf region based on wave age.

The aim herein is to describe inner shelf wind stress that is spectrally influenced by atmospheric winds traveling across the wave shoaling region and to evaluate the relevance of sea and swell wave contributions. The S09 and H15 models are proposed with slight modifications accounting for water depth dependence in the shoaling region. Simple models allow for more clarity in understanding of the physics than complex numerical models, as the terms and their magnitude can be compared and described easily. Average conditions for model inputs are focused on Monterey Bay (MB) climatology. S09 and H15 are compared to highlight similarities and differences and the water depths that result in fundamental changes are described.

A. S09 MODEL

An analytical model described by Semedo et al. (2009) (S09) for a constant flux layer is summarized starting with MOST (without waves). MOST is derived from classical turbulent theory where turbulent fluxes (in a statistically neutral environment) flow down the mean gradient at a rate proportional to an eddy viscosity (Stull 1988). This approach is combined with the mixing length theory, which defines a characteristic distance (l) that a

parcel of air/fluid will travel while conserving its properties before mixing with the surrounding air/fluid. A first-order closure approximation is formulated describing how kinematic eddy viscosity (ν_T) increases with increasing shear $\left(\frac{d\bar{u}}{dz}\right)$ (turbulence intensity) and increasing l (the ability of turbulence to cause mixing)(Stull 1988):

$$\nu_T = l^2 \left|\frac{d\bar{u}}{dz}\right| \tag{1.16}$$

where $(\bar{u})$ is the mean wind speed, and (z) is the height above the sea surface. The mixing length is approximated by the dimensionless Von Karman constant (κ) as follows (Stull 1988):

$$l = \kappa z. \tag{1.17}$$

The eddy viscosity is assumed to vary linearly with height and is defined in terms of u_* (Semedo et al. 2009):

$$(\nu_T^l)_z = \kappa z u_*. \tag{1.18}$$

The turbulent wind stress (referred to as τ_{turb} in S09) is defined as:

$$\tau_{\text{wind}} = \rho_{atm} \left(\nu_T^l\right)_z \frac{d\bar{u}}{dz}. \tag{1.19}$$

For two-dimensional stationary flow with no horizontal gradients, shear stress in the turbulent boundary layer is determined constant based on conservation of momentum (Ortiz-Suslow et al. 2018):

$$\frac{d\tau_{\text{wind}}}{dz} = 0. \tag{1.20}$$

This is known as the constant stress layer where vertical fluxes remain constant with height forming the basis for MOST. Rearranging Eq. (1.19) gives the MOST profile in S09 form:

$$\frac{d\bar{u}}{dz} = \frac{\tau_{\text{wind}}}{(\nu_T)\rho_{atm}}. \tag{1.21}$$

Integrating Eq. (1.21) (or any form of the gradient wind profile) gives the log wind profile which allows for the wind profile to be solved analytically by calculating the mean wind $(\bar{u})$ at each height (z) from a known reference height (r) (Ortiz-Suslow et al. 2018):

$$U(z) = U(z_r) + \frac{\tau_{\text{wind}}}{(\nu_T)\rho_{atm}} \ln\left(\frac{z}{z_r}\right). \tag{1.22}$$

When $\bar{u}(z_r) = 0$, the effect of sea stress is accounted for via z_0, and the log wind equation becomes:

$$U(z) = \frac{\tau_{\text{wind,sea}}}{(\nu_T)\rho_{atm}} \ln\left(\frac{z}{z_0}\right). \tag{1.23}$$

With the inclusion of waves, Eq. (1.2), Eq. (1.23) can be re-written as:

$$\frac{d\bar{u}}{dz} = \frac{\tau_{\text{total}} - (\tau_{\text{wave}})_z}{(\nu_T^b)_z \rho_{atm}}. \tag{1.24}$$

The wave stress $(\tau_{\text{wave}})_z$ is defined as the sum of contributions from both swell (decay) and sea (growth) to the entire spectrum:

$$\left(\tau_{wave}\right)_z = \underbrace{\int_0^{n_p} \frac{\beta^d g S(n)}{sc} e^{-2kz} dn}_{Swell} + \underbrace{\int_{n_p}^{\infty} \frac{\beta^g g S(n)}{sc} e^{-2kz} dn}_{Sea} \tag{1.25}$$

where s is the density ratio of the atmosphere to the ocean:

$$s = \frac{\rho_{atm}}{\rho_{ocean}} = \frac{1.2 \text{ kg m}^{-3}}{1028 \text{ kg m}^{-3}}. \tag{1.26}$$

β are coefficients for decay $\left(\beta^d\right)$ or growth $\left(\beta^g\right)$ dictated by $\left(C_\beta\right)$:

$$\beta = C_\beta \omega s \left(\frac{u_*}{c_p}\right)^2 \tag{1.27}$$

where growth (C_β=16) attributes sea and decay (C_β=-32) attributes swell, with assigned values based on the observations made by Chen et al. (2019).

A new viscosity term (ν_T^b) that includes waves is described by S09 using a Turbulent Kinetic Energy (TKE) dependent eddy viscosity, derived from the TKE (b) equation as follows (Semedo et al. 2009):

$$b^2 = \left|\tau_{\text{total}}(\tau_{\text{total}} - \tau_{\text{wave}}) + l\sqrt{b}F_w\right| \tag{1.28}$$

where:

$$\frac{(\nu_T^b)_z}{\sqrt{\rho_{atm}}} = l\sqrt{b}. \tag{1.29}$$

Equation (1.28) is represented in Chen et al. (2019) as follows:

$$\left(\nu_T^b\right)_z^4 \left(l^{-4}\right)_z = \left|\tau_{\text{total}}(\tau_{\text{total}} - (\tau_{\text{wave}})_z) + (\nu_T^b)_z F_{wz}\right| \tag{1.30}$$

where the wave term $\left(F_{wz}\right)$ is defined as:

$$F_{wz} = -2\kappa c(\tau_{\text{wave}})_z. \tag{1.31}$$

MOST has two fundamental assumptions: 1) constant flux layer, Eq. (1.20), and 2) the length scale given by Eq. (1.17). S09 still assumes a constant flux layer, where the τ_{total}

remains constant over the vertical. For S09, τ_{total} is the sum of $\tau_{wind,sea}$ and τ_{wave}, which has a vertical dependence that varies expontentially (shown in Figure 2). Though S09 provides a non-constant flux model, it is unclear how $\tau_{wind,sea}$ and τ_{wave} truly varies vertically and with no observations to test against, the constant flux layer S09 model is the focus herein. This is also the form that was field validated by Chen et al. (2019). The analytical representation of τ_{wave}, defined by Eq. (1.25) is exponental (blue line, Figure 2), which results in $\tau_{wind,sea}$, also exponential (red line, Figure 2) by definition. Since $\tau_{wind,sea}$ is expontential and describes the velocity gradient in Eq. (1.24), the profile differs from the logrimatic profile by MOST. Furthermore, Eq. (1.29) replaces Eq. (1.17) removing the MOST length scale relationship. The S09 model, even though it assumes constant flux, deviates significantly from MOST until above the WBL. To highlight these differences, some idealized conditions as shown in S09 are described next.

For τ_{wave}, it is largest at the sea surface that exponentially decays and asymptotes around z=20 m. This is considered the height of the WBL. Chen et al. (2019) during low winds suggested the WBL extended to 30 m. The e-folding height is approximately z=5 m, which was suggested by Cifuentes-Lorenzen et al. (2018). Here the top of the WBL is assumed to be zero at z=30 m, and is considered when initating the S09 model. Above the WBL, the constant flux layer extends, and since $\tau_{total} = \tau_{wind,sea}$ the assumptions for MOST are valid again. The S09 model blends MOST above the WBL with the waves effects within the WBL.

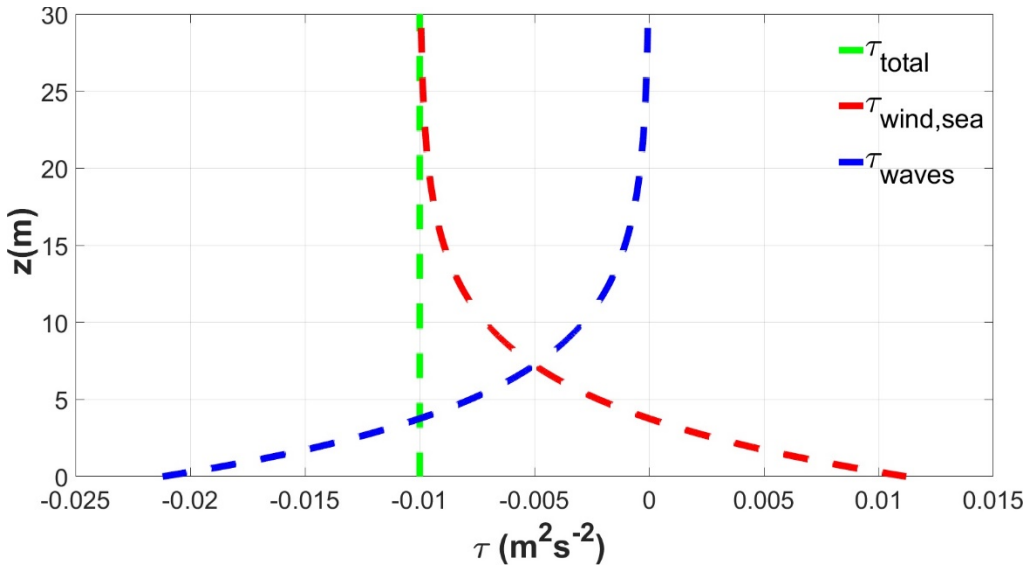

Figure 2. S09 constant stress model with τ_{total} = -0.1 m^2 s^{-2}, β = -5 x 10^{-5} s^{-1}, z_0 = 10^{-5} m, k = 0.1 m^{-1}, c_p = 9.9 m s^{-1}, and T = 6.3 s.

B. H15 MODEL

Högström et al. (2015) developed more of an empirical model (H15) that estimates u_* at 10 m when the wind and waves are both following and in the same direction for near-neutral atmospheric conditions using observations from several major field experimental datasets. H15 defines u_* as the summation of tangential stresses and form drag for both swell and sea as:

$$u_*^2 = \overbrace{\left(D_\tau\right)_{swell}}^{1} + \overbrace{\left(D_\tau\right)_{windsea}}^{2} + \overbrace{\left(D_{form}\right)_{windsea}}^{3} + \overbrace{\left(D_{form}\right)_{swell}}^{4}. \qquad (1.32)$$

Tangential Stress; Form Drag

Terms 1, 2 and 3 contribute positively to stress (downward momentum flux) and Term 4 contributes negatively (upward momentum flux). Högström et al. (2015) defines Term 1 to 4 as:

$$u_*^2 = \overbrace{1.25H_{sig,sw}^2 n_{peak}^2}^{1} + \overbrace{\left(C_D\right)_{wind,sea} U_{10}^2}^{2+3} - \overbrace{u_*^2 y}^{4} \qquad (1.33)$$

swell; wind+sea; swell

where Terms 2 and 3 in Eq. (1.33) are combined and represent the combined wind and sea portion (windsea), referred to as Term 2+3. H15 model is explicitly related to the parameter (*SF*), referred to as the swell factor given by:

$$SF = H_{sig,sw}^2 n_{peak}^2 \tag{1.34}$$

which is proportional to the magnitude of the orbital motion at the water surface. Högström et al. (2015) found a linear log-log relationship between *SF* and Term 1 in Eq.(1.33). The drag coefficient relation for pure sea is described as:

$$\left(C_D\right)_{wind,sea} = 10^{-3} \times (0.105 U_{10} + 0.167) \tag{1.35}$$

based on empirical observations from Drennan et al. (2003). The dimensionless parameter *y* in term 4 was obtained by linear regression that is valid for 0.5 m< $H_{sig,sw}$ <2.0 m:

$$y = 0.269 - 0.126 H_{sig,sw} \tag{1.36}$$

and for $H_{sig,sw}$ >2.0 m or $H_{sig,sw}$ <0.5 m:

$$y = 0. \tag{1.37}$$

Högström et al. (2015) stated that Eq. (1.36) was not dimensionally satisfactory but other relevant length dimensions were not empirically found. Eq. (1.33) can be rewritten for an expression of u_* as follows:

$$u_* = \sqrt{\frac{\left(C_D\right)_{wind,sea} U_{10}^2 + 1.25 H_{sig,sw}^2 n_{peak}^2}{1+y}}. \tag{1.38}$$

Högström et al. (2015) also stated that their model developed on the range of *SF* is typical of conditions found seasonally across the globe based on summaries provided by Semedo et al. (2009) and Semedo et al. (2011). They noted missing measurements needed to cover the full range of conditions are on the upper tail end of *SF*, and when C_D >2. For

the inner shelf, *SF* increases with decreasing depth where C_D has been observed to be greater than 2.

II. METHOD

A. MODEL INPUT REPRESENTATION

H_{sig} and T_p (peak period) are obtained from MB National Data Buoy Center (NDBC) Station 46114 from Sep 2011–Dec 2019 (Figure 3). H_{sig} ranged from 0.5–10 m that seasonally varies (Figure 3a), with a mean 2.17 m and a median of 1.97 m. T_p ranged from 3.5–25 s with a mean 12.1 s (Figure 3b). The range of U was obtained from NDBC Station 46092 from Dec 2008–Dec 2019 and ranged from 0–24 m s^{-1}, with an average of 5 m s^{-1}. Hourly wave spectra, $S(n)$, are also provided by NDBC Station 46042 from 2005–2019 (Figure 4) with n_{peak} = 0.08 Hz. These climatological conditions define the range of conditions implemented for the offshore boundary of the model.

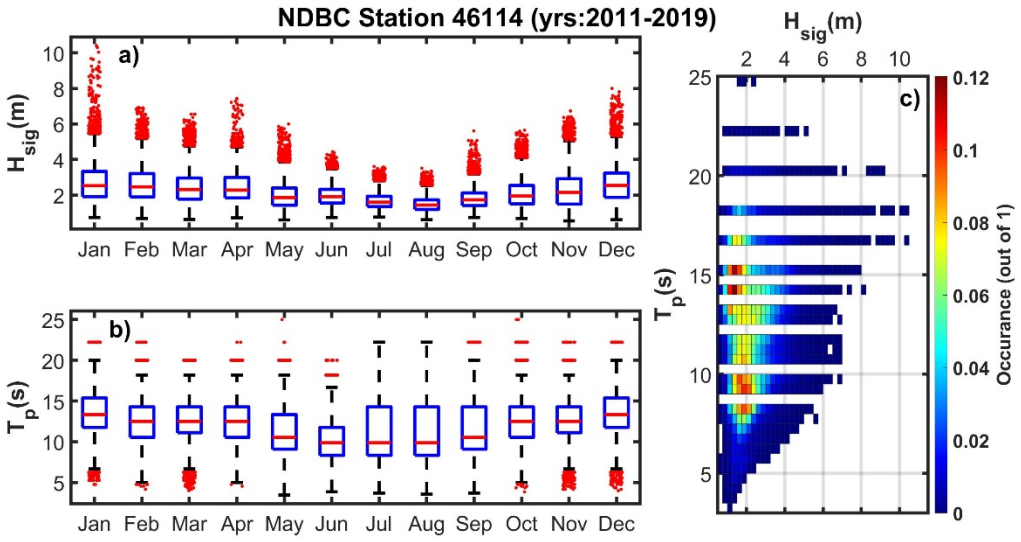

Figure 3. MB NDBC wave data. With a) H_{sig} seasonal variations and b) T seasonal variations where the central line of the box represents the median, the bottom and top edges the 25th and 75th percentiles, the whiskers indicate the most extreme data points, and the red dots represent outliers. T and H_{sig} occurrences c) are shown as a fraction of 1.

B. SPECTRAL WEIGHTS

The goal herein is an evaluation of wind and wave contributions to wind stress (or u_*) and how it varies across the inner shelf. To reduce the number of input variables for clarity in response, a spectral weight is developed and applied to the bulk statistic of H_{rms} for both models. When wave energy spectra are not available, S09 and Chen et al. (2019) used a parametric spectrum that depends on U_{10} and can be modified for *h*. It was recognized that this type of spectrum does accurately account for swell. Here a characteristic spectrum is defined, which is the average of the hourly spectra described as:

$$S_{norm}(n) = \frac{\langle S(n) \rangle}{\int_0^\infty \langle S(n) \rangle dn} \tag{2.1}$$

divided by the integral of $S(n)$ such that that variance is normalized to 1, where brackets represent time average (Figure 4). $S_{norm}(n)$ is relatively broad-banded spanning 0.05 to 0.2 Hz, with n_{peak} at 0.08 Hz (Figure 4). The spectral weights, γ, for sea and swell (superscripts) are defined as:

$$\gamma_{sw} = \int_0^{n_p} S_{norm}(n) dn \tag{2.2}$$

$$\gamma_{sea} = 1 - \gamma_{sw}. \tag{2.3}$$

Since n_p is dependent on *h* and U_{10}, γ is also dependent on *h* and U_{10} and varies accordingly. A second weighting category is defined using the deep water relationship (subscript o) for c_p (Eq.(1.11)) for both swell, $\gamma_{sw,o}$ and sea, $\gamma_{sea,o}$ to enable a comparison to the original S09 and H15 approaches. The spectral weights are applied to the bulk H_{rms} to appropriately account for the spectral distribution of sea and swell, where Eq (1.14) and (1.15) are re-written to incorporate the spectral weights as follows:

$$H_{rms,sw} = \gamma_{sw} H_{rms} \simeq 2\sqrt{2}\sqrt{\int_0^{n_p} S(n)\,dn} \tag{2.4}$$

$$H_{rms,sea} = \gamma_{sea} H_{rms} \simeq 2\sqrt{2}\sqrt{\int_0^{\infty} S(n)dn}. \tag{2.5}$$

The total wave variance is defined as:

$$\sigma^2 = \left(H_{rms} \Big/ 2\sqrt{2} \right)^2 \tag{2.6}$$

where σ^2 is variance. With this characteristic spectrum, Eq. 1.25 can be re-written as:

$$\left(\tau_{wave}\right)_z = \underbrace{\int_0^{n_p} \frac{\beta^d g S_{norm}(n)\sigma^2}{sc} e^{-2kz} dn}_{Swell} + \underbrace{\int_{n_p}^{\infty} \frac{\beta^g g S_{norm}(n)\sigma^2}{sc} e^{-2kz} dn}_{Sea}. \tag{2.7}$$

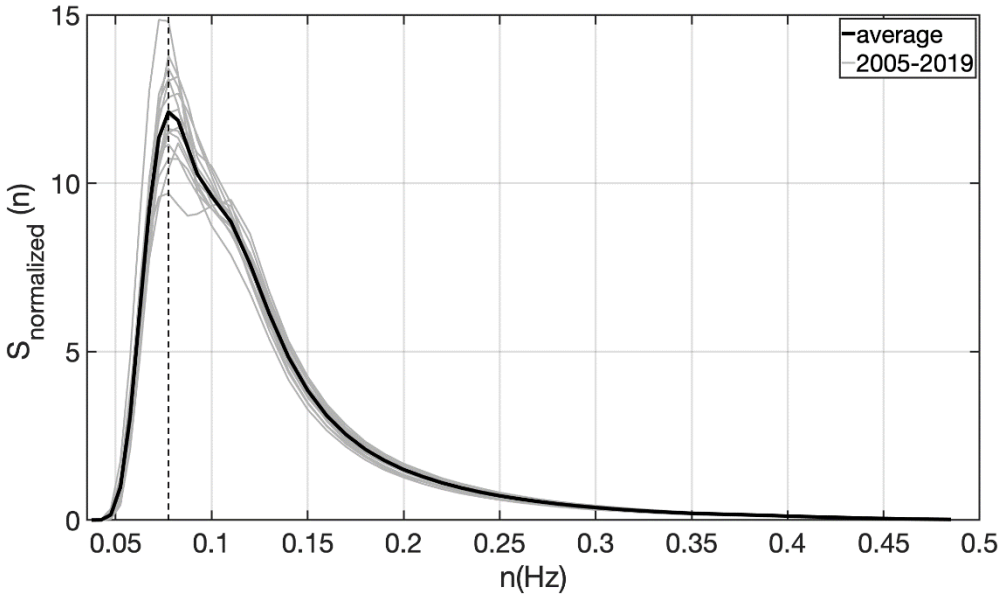

Figure 4. Normalized energy density spectrum from MB NDBC Station 46042 averaged from hourly observations over the period 2005–2019.The vertical black dashed line represents n_{peak} = 0.08 Hz.

C. WAVE SHOALING

H_{rms} is shoaled across water depths excluding refraction and diffraction (i.e., waves are normally incident), without any losses due to bottom friction, and ignoring reflection (Reeve 2018). Shoaling H_{rms} from one depth to another depth is described as:

$$H_{rms,2} = K_s H_{rms,1} \tag{2.8}$$

where subscripts represent the values at the two depths, and the shoaling coefficient, K_s, is:

$$K_s = \sqrt{\frac{c_{g,1}}{c_{g,2}}} = \sqrt{\frac{\frac{c_{p,1}}{2}\left(1+\frac{2kh_1}{\sinh 2kh_1}\right)}{\frac{c_{p,2}}{2}\left(1+\frac{2kh_2}{\sinh 2kh_2}\right)}} \tag{2.9}$$

where c_g is the group velocity. When $H_{rms} < 0.42h$, wave breaking occurs (Thornton and Guza 1983). H_{rms} is described at the offshore boundary at *h*=30 m $\left(H_{30}\right)$ and shoaled onshore into shallower water depths. Note c_p, Eq. (1.12), is also shoaled across water depths.

D. VELOCITY PROFILE DIFFERENCES: IMPACTS ON CD

C_D from field observations is commonly computed as:

$$C_D(z) = \frac{\tau_{obs}(z)}{\rho_{atm} U_{obs}^2(z)} = \frac{\overline{u'w'}(z)}{U_{obs}^2(z)} \tag{2.10}$$

where at height *z* (generally at 10 m), $\overline{u'w'}(z)$ is estimated with a sonic anemometer using eddy-covariance (Edson et al. 1998), and $U_{obs}(z)$ is the mean wind at the same elevation. Here, it assumed that $\tau_{obs}(z)$ includes both wind and waves contributions, can is also defined as τ_{total}:

$$\tau_{\text{total}}(z) = \tau_{obs}(z) = \tau_{\text{wind}}(z) + \tau_{\text{wave}}(z). \tag{2.11}$$

In the field, there is no explicit method to separate τ_{wind} and τ_{wave} with standard observations. Therefore, C_D is suggested to include contributions by wind and waves. However, S09 demonstrates that the $U(z)$ is also modified by the presence of waves. Since both $\tau_{obs}(z)$ and $U_{obs}(z)$ include the influence of waves, this may result in offsetting biases that result in cancelling the net wave effects in C_D. Here, C_D is evaluated at 10 m using two models, described as $U_{no-waves}(10)$ (no waves) and $U_{waves}(10)$ (with waves), and using the *same* $\tau_{obs}(10)$ by Eq. (1.9). The $\tau_{\text{wind,sea}}$ elements only are compared from each model to evaluate the effect of considering wave stress. The process for evaluating each profile is the same, however, $U_{no-waves}$ considers $\tau_{\text{wave}} = 0$, and therefore, $\tau_{\text{wind,sea}} = \tau_{obs}$, and uses the linear eddy viscosity $\left(\nu_T^l\right)_z$. For U_{waves}, $\tau_{\text{wave}} \neq 0$, $\tau_{\text{wind,sea}} = \tau_{obs} - \tau_{wave}$, and uses the TKE eddy viscosity $\left(\nu_T^b\right)_z$.

$U_{no-waves}(z)$ is computed using the law of the wall Eq. (1.3) with z_0 based on Charnock, where u_* is:

$$u_* = \sqrt{\left|\frac{\tau_{obs} - \tau_{\text{wave}}}{\rho_{atm}}\right|}. \tag{2.12}$$

Eq. (1.3) can be solved directly for $U_{no-waves}(z)$. For waves, $U_{waves}(z)$ is computed using the S09 model, where Eq. (1.21) is numerically estimated by a top-down forward difference method described as:

$$U_2 = U_1 + \frac{\tau_{obs} - \tau_{\text{wave}}(z)}{(\nu_T^b)_z \rho_{atm}}(z_2 - z_1). \tag{2.13}$$

Note both $\tau_{\text{wave}}(z)$ and ν_T^b vertically vary as descrbed in Eqs. (1.25) and (1.29). $U_{waves}(z)$ (S09 model) is initiated at *z*=30 m to be well above the WBL (Chen et al. 2019) by using $U_{no-waves}(z)$ computed at 30 m. At z=10 m, $C_{D,no-waves}$ and $C_{D,waves}$ are computed using:

$$C_{D,XXXX} = \frac{\tau_{obs,XXXX}}{\rho_{atm} U_{XXXX}(z)^2_{obs,XXXX}} \tag{2.14}$$

where XXXX subscript is either no waves or waves. τ_{obs} will vary based on common observed stress found over the inner shelf (Fewings and Lentz 2010), and C_D will be evaluated using $U_{no-waves}$ and U_{waves}.

E. STRESS BALANCE ACROSS THE INNER SHELF

Both S09 and H15 have contributing terms for wind and wave in defining the wind stress. A stress balance is performed to evaluate the magnitude of the stress terms and their variation from 30 to 5 m water depth (i.e., the inner shelf). Three scenarios are compared for the H15 analysis to determine the magnitude and spatial variation of each term in response to shoaling. Scenario 1, 'all-shoal' evaluates H_{30} shoaled to determine H_{rms} and c_p accounting for shoaling using n_p and the γ_{sw} weighting function. Scenario 2, 'H-constant' evaluates H_{30} as constant with c_p shoaled using n_p and the γ_{sw} weighting function. Scenario 3, 'no-shoal' has no shoaling effects considered, evaluates H_{30} as constant and uses the deep water relationship to calculate c_p and the $\gamma_{sw,o}$ spectral weighting. Only the 'all-shoal' scenario is used to compare S09 and H15 terms together due to the limited impact of the S09 swell term.

The wave contributions will vary for the 'all-shoal' and 'H-constant' scenarios because c_p varies across these depths, and this defines n_p for determining whether the wave contribution is either sea (positive contribution) or swell (negative contribution). Sea and swell are primarily related to $\gamma(u,h)$, a uniform distribution that is weighted by the

influence of both $\boldsymbol{n_p}$ and $S_{norm}(n)$. This will provide an inherent description of how sea and swell are defined across the inner shelf, which is independent of H_{rms} and corresponding wave stress terms. The stress balance for S09 and H15 herein, uses H_{rms}, U_{10}, and *h* as varied inputs, and uses $S_{norm}(n)$ as constants. Using these inputs, the stress balalance is evalauted and compared across the inner shelf.

THIS PAGE INTENTIONALLY LEFT BLANK

III. RESULTS

A. SPECTRAL WEIGHTS AND FACTOR

The contribution of sea and swell across the inner shelf is dependent on c_p which varies as function of frequency (n) and depth (h). The combined sea swell frequency band is defined as n=0.04–0.29 Hz based on the NDBC spectral range. In general, c_p decreases across the inner shelf (h=5-30 m) for the sea swell frequency band (Figure 5). The decrease in c_p is larger for lower frequencies and start at h=30 m, where c_p for the high frequencies have minimal changes and only start to decrease for h<10 m. The range of c_p is largest in deep water and reduces with decreasing water depths. This is the well-known linear wave theory response in describing c_p as per Eq. (1.12). This is fundamental in determining when $U_{10} = 1.14 c_p$ and therefore $\boldsymbol{n_p}$, for separating sea and swell contributions (Figure 6).

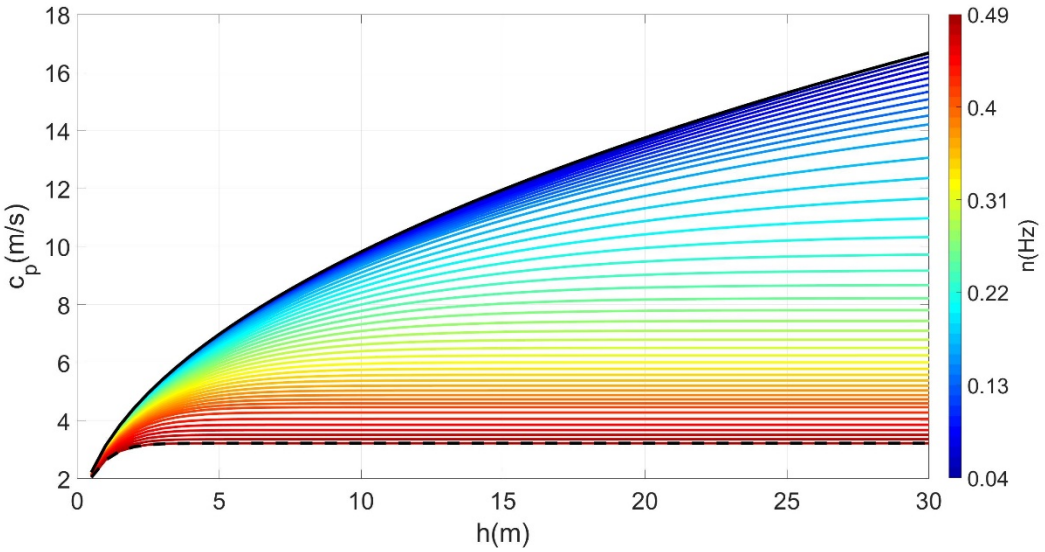

Figure 5. Wave phase speed $\left(c_p\right)$ vs depth (h) using the full dispersion relation for depths (h) 3–30 m based on the MB NDBC spectral range.

Using c_p (Figure 5), the transition frequency, n_p, is evaluated as per Eq. (1.13) across the inner shelf for different U_{10} (Figure 6). For U_{10} <3 m s^{-1}, the spectra across *h* and *n* are mostly described as swell conditions. For U_{10} >13 m s^{-1}, the spectra across *h* and *n* are mostly described as sea conditions. For U_{10} =4-13 m s^{-1}, the spectra across *h* and *n* represent both sea and swell conditions that vary. With increasing U_{10} from 4 to 13 m s^{-1}, the transition from swell to sea conditions occurs first at shallower depths and at high frequencies. With each increase in U_{10}, the sea contribution increases and the swell contribution decreases. This can be summarized as three regimes for the inner shelf, swell-dominated (U_{10} <3 m s^{-1}), mixed (U_{10} =4-13 m s^{-1}), and sea-dominated (U_{10} >13 m s^{-1}).

The transition frequency is also evaluated using the deep water relationship, c_o (Eq. (1.11) (Figure 6, white dashed line). c_o remains constant with *h*, and for U_{10} <4 m s^{-1} is equivalent to n_p for all *h*. For the mixed sea swell regime, c_o is equivalent to n_p offshore, but deviates in shallow regions with increasing U_{10} up to ~11 m s^{-1}. The deviation between c_o and n_p occurs at *h*=15 m at the upper limit of the mixed sea swell regime, no values align once entering the sea dominated regime (U_{10} >12 m s^{-1}). This indicates that the largest differences when accounting for shoaling c_p, via the evaluation of n_p, occurs predominantly in *h*<15 m and for U_{10} <12 m s^{-1}.

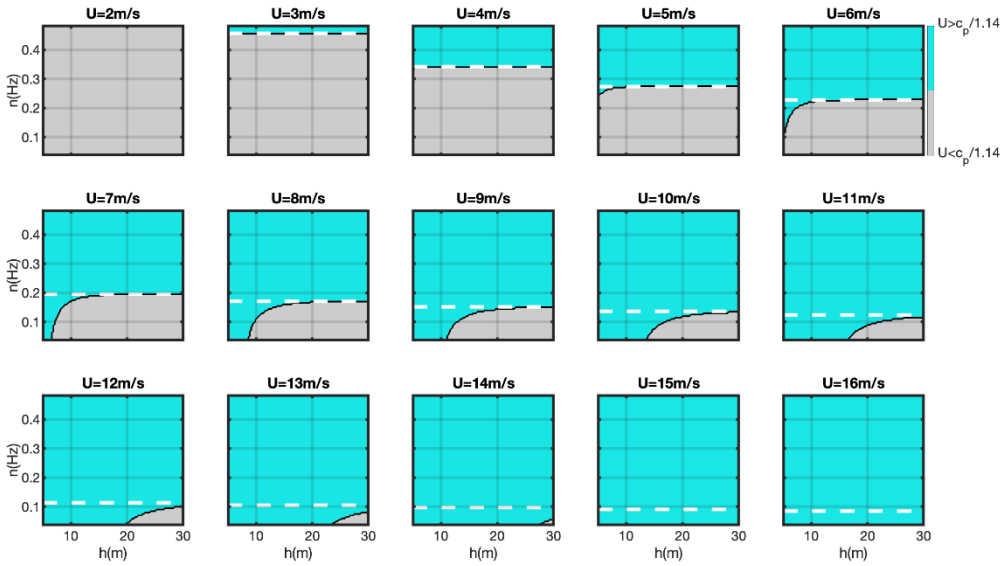

Figure 6. Evaluation of sea (aqua, growth) and swell (grey, decay) based on the MB wave spectral frequencies (n), winds at 10 m (U), and the transition frequency, n_p. The transition frequency using the deep water relationship is indicated by the white dashed line.

γ spectrally weights (Figure 6) based on the characteristic energy density spectrum (Figure 4). Since γ is a spectral integral, it can described as function of h and U_{10} (Figure 7). Based on the three regimes, γ transitions from swell to mixed to sea, where γ_{sw} (γ_{sea}) will be 1 (0) in swell, a fraction (fraction) in mixed, and 0 (1) in sea. In Figure 6, the mixed regime occurred for U_{10} =4-13 m s^{-1} but γ_{sw} is also senstive to the spectral shape. This results in the γ_{sw} transition gradients (Figure 7) being less binary than those shown in Figure 6. The winds that highlight transitional γ_{sw} support a smaller range, and occur for U_{10} =6-11 m s^{-1} (Figure 7a). The transitional range supports a sharp gradient (<1 m s^{-1}) at shallow water depths (h<6 m), where the gradient increases to an asymptotic limit (~6 m s^{-1}) at ~15 m water depth (Figure 7a). This is because the characteristic spectrum has minimal energy at n<0.07 Hz (Figure 4) and the swell contributions for lower frequencies are nearly zero. As stated above, open-ocean C_D formulations generally work

in sea conditions. Mixed and swell conditions are of revelance herein, and occur when U_{10} <10 m s^{-1} and the largest differences in response occur for inner shelf depths < 15 m.

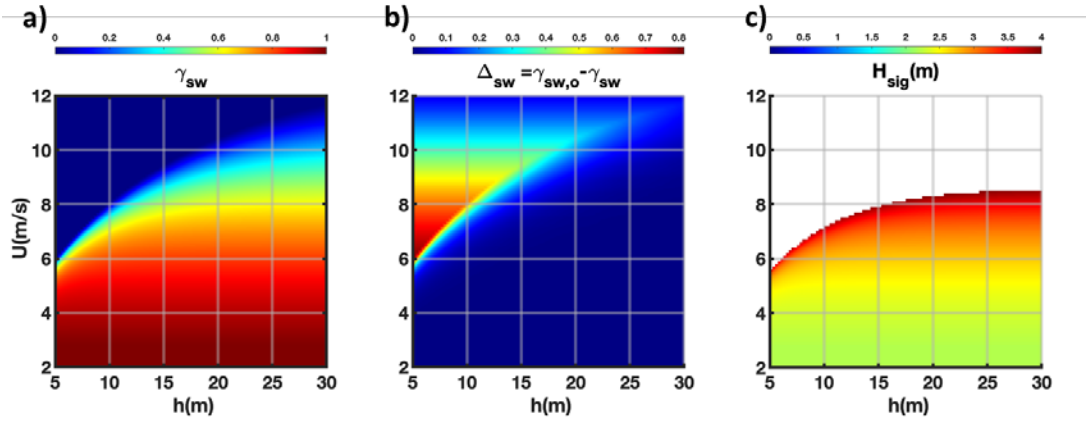

Figure 7. Swell spectral weight (γ_{sw}) (a).The difference between the deep water swell spectral weight $(\gamma_{sw,o})$ and γ_{sw} (b). The maximum H_{sig} that can be resolved by H15 limited by an 80% probability of occurance from MB climatology of 4 m (c).

B. S09 VELOCITY PROFILES AND CD IMPACTS

The impact of considering waves on $U(z)$ and C_{D10} is evaluated using S09. Two wind profiles are evaluated based on τ_{turb}, $U_{no-waves}$ and U_{waves}, using the single wave test parameters (Figure 2), and single observed stress of -0.01 m^2 s^{-2} at 10 m (Figure 8). Waves reduce stress at z=10 m by 25%, corresponding to a 25% increase in $C_{D10,waves}$ compared to $C_{D10,no-waves}$. The impact of waves on $U(z)$ is most significant near the surface (z=0) where a maximum U velocity is observed, and decreases with height until intersecting with $U_{no-waves}$ at ~z=2 m. The impact of waves continues to be observed throughout the vertical up to $U(30)$, but decreases with increasing (z) and tends towards the logarithmic profile exhibited by $U_{no-waves}$ in response to the wave effects reducing with height.

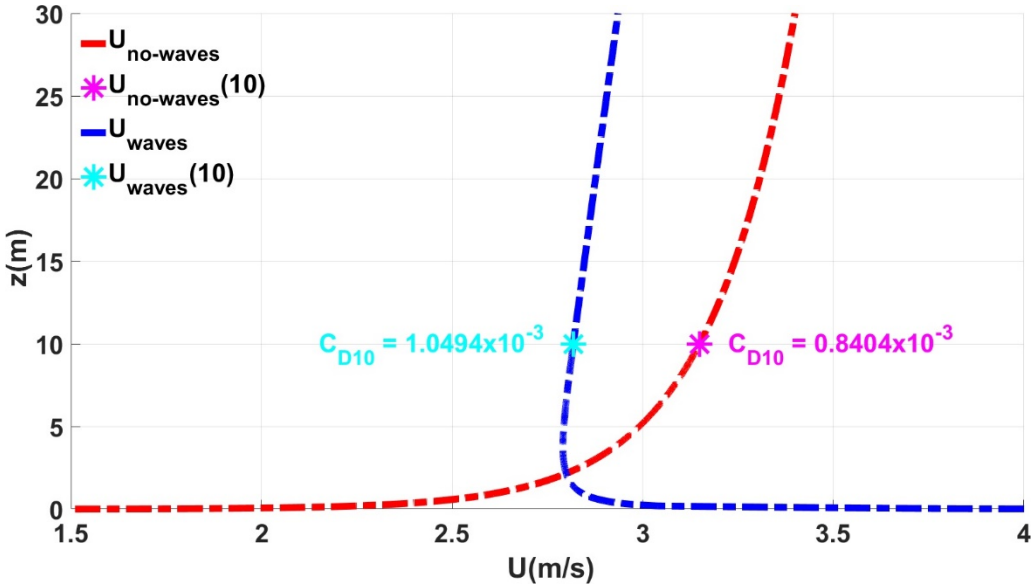

Figure 8. $U_{no-waves}$ (red dashed) and U_{waves} (blue dashed) with τ_{obs} = -0.01 $m^2\ s^{-2}$ at 10 m, the Charnock estimate for z_0, and initiating the model at $U(30)$. C_D evaluated at 10 m for $U_{no-waves}$ (magenta) and U_{waves} (cyan).

As τ_{obs} increases for the same single τ_{wave} as in Figure 8, the wave influence reduces and U_{waves} trends towards a logarithmic profile (Figure 9a). As $\tau_{wind,sea}$ increases for larger τ_{obs} the difference in C_D between U_{waves} and $U_{no-waves}$ reduces due to τ_{wave} remaining constant and the wind effects oversaturating the wave effects (Figure 9b). S09 τ_{waves} influence $U(z)$ throughout the vertical, with the largest effects observed at lower τ_{obs} and z=0, reducing with increasing τ_{obs} and increasing z.

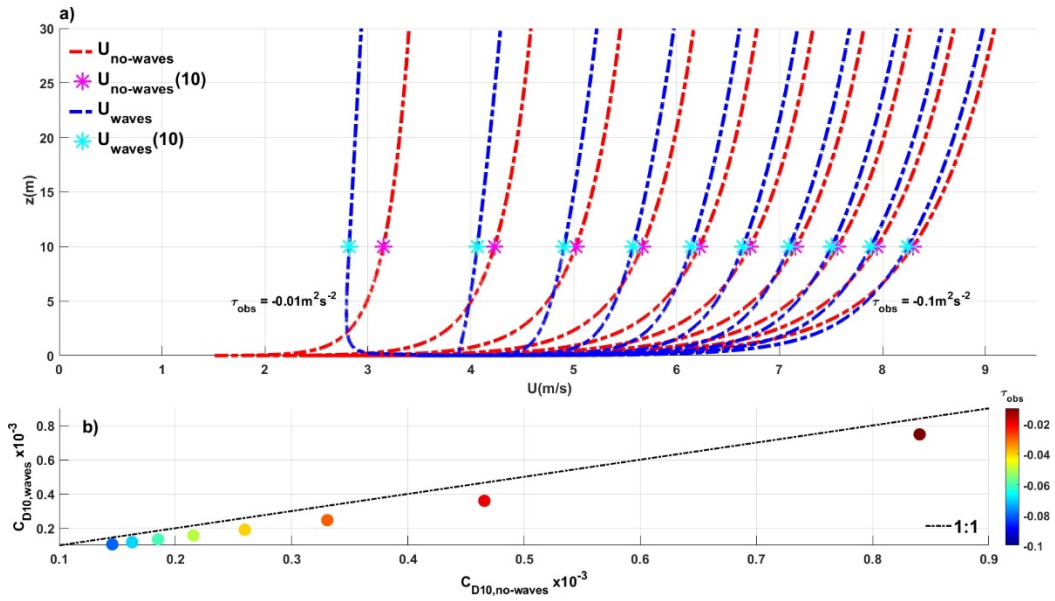

Figure 9. S09 wind profiles $U_{no-waves}$ (red dashed), U_{waves} (blue dashed) with varying τ_{obs} at 10 m from -0.1 m^2s^{-1} to -0.01 m^2s^{-1} (a) and corresponding C_D values at 10 m (b).

C. STRESS BALANCE

H15 and S09 wind and wave stress terms ($\boldsymbol{u_*}$) are evaluated and their evolution across the inner shelf. For the evaluation, $\boldsymbol{H_{sig}}$ values of 0.5 and 1.5 m are applied at the offshore boundary in 30 m water depth. The reason for these wave heights is that they represent the upper and lower limits of H15 (Eq. (1.36)) T4, which is defined for $0.5 < H_{sig,sw} < 2.0$ m, whereas outside of this limit T4 provides zero contribution. Though T1 in H15 has no upper $\boldsymbol{H_{sig}}$ limit, it is influenced by γ_{sw} (as will be shown below), which tends to limit the acceptable range of H_{sig} and therefore these two $\boldsymbol{H_{sig}}$ values are deemed appropriate. For H15, the swell wave terms (T1+T4, Eq.(1.33)) and the wind and sea terms (T2+T3, Eq. (1.33)) are combined and will be referred to as $u_{*\text{wave,sw}}$ and $u_{*\text{wind,sea}}$. Since $u_{*\text{wind,sea}}$ is independent of water depth, it increases linearly with U_{10} and ranges from 0 to 0.4 m s^{-1} for U_{10} =0-12 m s^{-1} (Figure 10a, 11a). $u_{*\text{wave,sw}}$ is dependent on water depth, and is

a function of $H_{sig,sw}$, n_p, and $u_{*\text{wind,sea}}$. The question is how much $u_{*\text{wave,sw}}$ varies. Three scenarios are described to highlight the depth influence of wave shoaling across varying water depths on H_{sig} and c_p for defining n_p. These scenarios are: 1) both c_p and H are shoaled ('all-shoaled') (Figure 10bc, 11bc), 2) c_p is shoaled, H remains constant as defined at the offshore boundary ('H-constant') (Figure 10de, 11de), and 3) c_o is based on the deepwater relationship that is independent of h, so that H_{sig} remains constant as defined at the offshore boundary ('no-shoal') (Figure 10fg, 11fg). For H_{sig} = 0.5 m, $u_{*\text{wave,sw}}$ varies on h and U, but it is relatively minimal (Figure 10bdf) when compared to $u_{*\text{wind,sea}}$ (Figure 10a). There are differences amongst the three scenarios (Figure 10bdf) and these trends are similar to when H_{sig} increases to 1.5 m (Figure 11bdf), except now $u_{*\text{wave,sw}}$ is of equal significance relative to $u_{*\text{wind,sea}}$ (Figure 11a). The discussion will focus on H_{sig} =1.5 m owing to larger $u_{*\text{wave,sw}}$ contributions.

The effects of shoaling H_{sig} are continuous, as $u_{*\text{wave,sw}}$ increases with decreasing depth (Figure 11b) and increasing H_{sig} (not shown). For h=30 to h=5 m, there is approximately a 50% increase in $u_{*\text{wave,sw}}$ when U <5 m s^{-1}. The effects of shoaling H_{sig} reduces the depth variability in $u_{*\text{wave,sw}}$ at larger U, but for U>6 m s^{-1} the γ_{sw} (Figure 7a) mixed sea swell region starts to influence the $u_{*\text{wave,sw}}$ contributions (Figure 11b).

$u_{*\text{wave,sw}}$ is positive at low winds and transitions to slightly negative (Figure 11b) in the transition region shown in γ_{sw} (Figure 7a). Without shoaling H_{sig}, the depth dependence is reduced as $u_{*\text{wave,sw}}$ is relatively constant across depth (Figure 11d), except for the influence of γ_{sw} (Figure 7a). This results in an underestimate of $u_{*\text{wave,sw}}$ for shallower depths. As expected, removing all depth dependence (Figure 11f), results in a uniform distribution from h=30 m to h=5 m. This results in an underestimate of $u_{*\text{wave,sw}}$ for shallower depths and U<6 m s^{-1}, and an overestimate of $u_{*\text{wave,sw}}$ for shallower depths

for U> 6 m s^{-1}, similar to $\gamma_{sw,o}$ (Figure 7b). For H_{sig} =1.5 m, $u_{*\mathrm{wave,sw}}$ are important as they are large enough to modify the total u_* up to U=10 m s^{-1} (Figure 11c). These scenarios highlight the H15 dependence on H_{sig}, where increasing H_{sig} increases $u_{*\mathrm{wave,sw}}$ (compare Figure 10 to 11), and therefore shoaling H_{sig} is important (Figure 11b). The combination of shoaling H_{sig} and γ_{sw} significantly changes $u_{*\mathrm{wave,sw}}$ (compare Figure 11bdf).

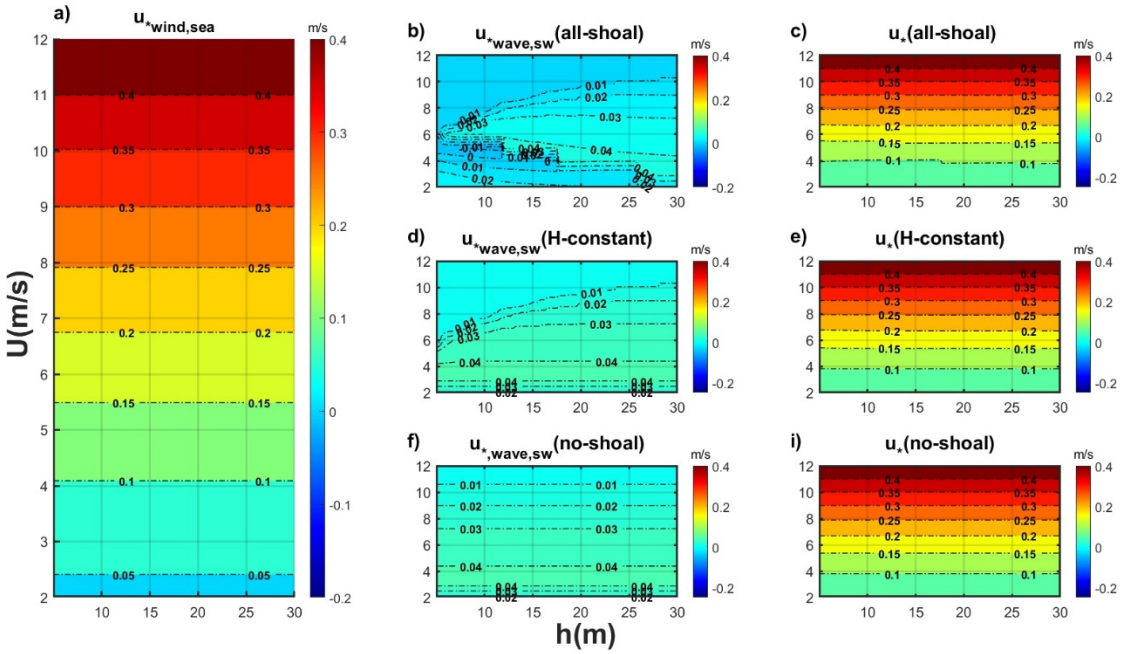

Figure 10. H15 term comparison from Eq. (1.33) for H_{sig} = 0.5 m between $u_{*\mathrm{wind,sea}}$ (Term 2+3) (a), and swell $u_{*wave,sw}$, (Term 1 and Term 4) (b,d,f) and the total u_* (c,e,i) for all-shoal, H-constant, and no-shoal scenarios respectively over the shoaling region for U_{10} =2-12 m s^{-1}.

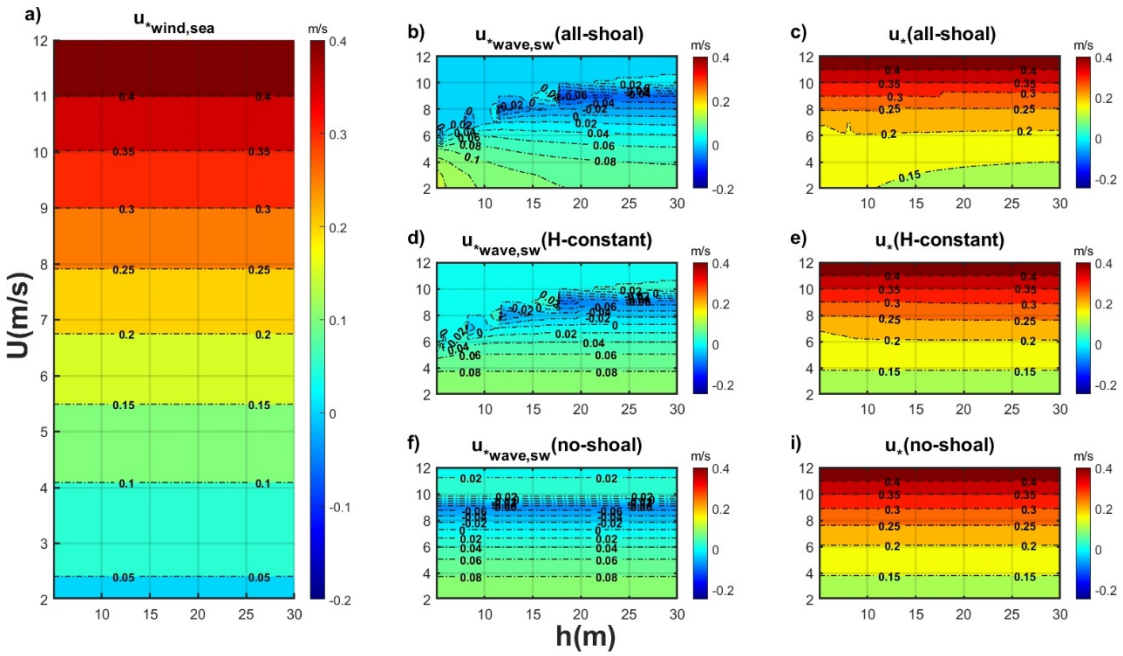

Figure 11. H15 term comparison from Eq.(1.33) for H_{sig} =1.5 m between $u_{*\mathrm{wind,sea}}$ (Term 2+3) (a), and swell $u_{*wave,sw}$, (Term 1 and Term 4) (b,d,f) and the total u_* (c,e,i) for all-shoal, H-constant, and no-shoal scenarios respectively over the shoaling region for U_{10} =2-12 m s^{-1}.

H15 swell T1 and T4 terms from Eq. (1.33) are competing as one provides a positive $u_{*\mathrm{wave,sw}}$ and one provides a negative $u_{*\mathrm{wave,sw}}$. Both terms are dependent on H_{sig} and, therefore, dependent on *h*. Only the shoaled scenario is evaluated for H_{sig} =0.5 m (Figure 12abc) and H_{sig} =1.5 m (Figure 12def). For T1, shoaling H_{sig} results in the largest positive values that increase with decreasing *h* and decreasing *U* (Figure 12ad). The trend is identical, the $u_{*\mathrm{wave,sw}}$ magnitude differs between H_{sig} =0.5 m and H_{sig} = 1.5 m (Figure 12ad). It is important to note the T1 term has no true limitation; here it can be seen to be limited by applying γ_{sw} to H_{sig}. T4 is much more complex in its pattern (12be). For H_{sig} =0.5 m, T4 does exist for larger *U* below γ_{sw} limitation (Figure 12b), whereas for H_{sig} =1.5 m it extends to γ_{sw} limitation (Figure12e). In general, it decreases to a larger negative value with decreasing depth and increasing *U*. The T4 trend is opposite to T1, and the net

is complex when H_{sig} =0.5 m (Figure 12c) with complexity isolated for when the gradient γ_{sw} is largest (Figure 7a) and for H_{sig} =1.5 m (Figure 12f).

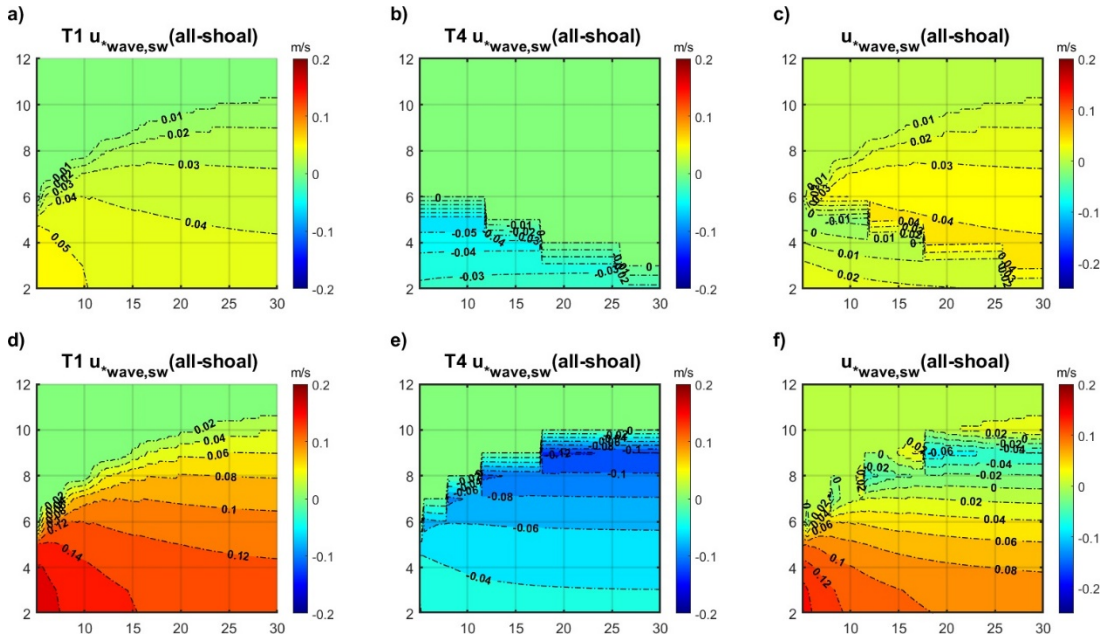

Figure 12. H15 term comparison from Eq. (1.33) for $H_{sig} = 0.5$ m (a,b,c) and $H_{sig} = 1.5$ m (d,e,f) between swell terms Term 1 (growth) (a,d) and Term 4 (decay) (b,e) to the total $u_{*\mathrm{wave,sw}}$ (c,f) for all-shoal conditions over the shoaling region for U_{10} =2-12 m s^{-1}.

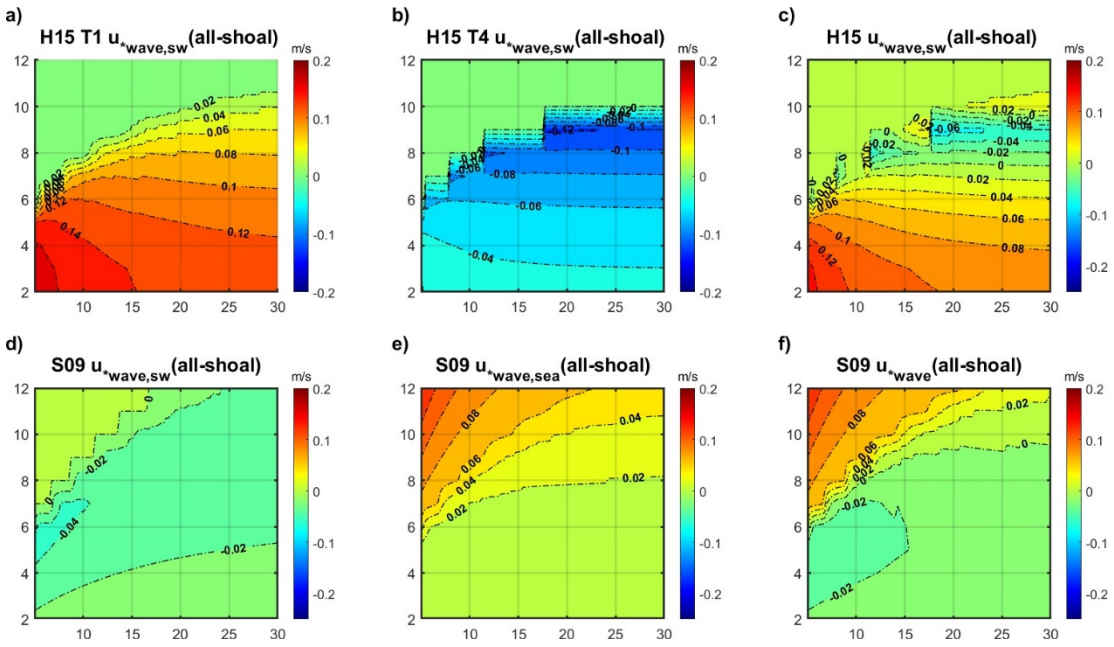

Figure 13. All-shoal conditions for H_{sig} =1.5 m comparing H15 T1 (growth) (a) and T4 (decay) (b) to the total $u_{*\mathrm{wave,sw}}$ (c). S09 swell (decay) (d) and sea (growth) (e) terms to the total wave stress (f).

The H15 and S09 $\boldsymbol{u_{*\mathrm{wave}}}$ are compared for differing *h* and *U* using $H_{sig} = 1.5$ m (Figure 13). As shown above, H15 has positive and negative contribution of $u_{*\mathrm{wave,sw}}$ (Figure 13 a,b), where S09 has only negative $u_{*\mathrm{wave,sw}}$ (Figure 13d). H15 has no explicit $\boldsymbol{u_{*\mathrm{wave,sea}}}$ instead it has positive contributions by $\boldsymbol{u_{*\mathrm{wind,sea}}}$(T2+T3 in Eq.(1.33), shown in Figure 10a, 11a). S09 has an explicit $\boldsymbol{u_{*\mathrm{wave,sea}}}$which is only positive (Figure 13e) and continues to increase with increasing U_{10}. For the swell $u_{*\mathrm{wave,sw}}$, H15 (Figure 13c) and S09 (Figure 13d) are significantly different, where S09 $u_{*\mathrm{wave,sw}}$ is relatively small and negative and H15 $u_{*\mathrm{wave,sw}}$ is large and positive. The net effect of S09 (Figure 13f) is mostly described by $\boldsymbol{u_{*\mathrm{wave,sea}}}$and $u_{*\mathrm{wave,sw}}$ is negligible. It hypothesized that H15 accounting for $\boldsymbol{u_{*\mathrm{wave,sea}}}$in $\boldsymbol{u_{*\mathrm{wind,sea}}}$is appropriate. However, S09 $\boldsymbol{u_{*\mathrm{wave,sea}}}$ should not be included as this will lead to doubling the influence of $\boldsymbol{u_{*\mathrm{wave,sea}}}$when combined with $\boldsymbol{u_{*\mathrm{wind,sea}}}$, which is already described

as $u_{*\mathrm{wind}}$ for the open ocean. Even though S09 provides a theoretical description over the vertical, S09 $u_{*\mathrm{wave,sw}}$ will always be negative and H15 $u_{*\mathrm{wave,sw}}$ will mostly be positive, and unfortunately there is no clear relationship between the two models. Based on the H15 development on various field observations, it is believed that H15 is the more representative of reality.

IV. DISCUSSION

It was hypothesized that higher observed wind stress across the inner shelf was due to wave dependence on water depth in shoaling regions. Two models validated for deep water, were modified for depth dependence, and analyzed across a shoaling region, h=5-30 m, to represent the inner shelf (outside breaking to ~11km off the coastline). The H15 model revealed that by accounting for shoaling (via c_p and H varying with depth) and spectrally accounting for sea and swell contributions that also vary with depth, swell wave stress can be up to 50% higher inshore (h=5 m) compared to offshore (h=30 m) for U<6 m s^{-1} (Figure 12f). Based on MB climatology and the transition frequency (n_p), three regimes were firstly identified being swell dominated (U_{10} <3 m s^{-1}) mixed sea swell transition (U_{10} =4-13 m s^{-1}) and sea dominated (U_{10} >13 m s^{-1}) (Figure 6). Comparison to the deep water relationship for wave phase velocity (c_o) revealed that the largest differences when shoaling c_p (via the evaluation of n_p) occur predominantly in h<15 m and for U_{10} <12 m s^{-1} (Figure 6). The spectral weight based on the MB energy density spectrum fully describes swell conditions for U_{10} <6 m s^{-1} (Figure 7a). The largest difference in spectral weight for swell in comparison to the deep water relationship occur for U_{10} =6-10 m s^{-1} and h<15 m (Figure 7b). These regions correlate to where stress estimates vary when shoaling is considered. By not shoaling H_{sig}, stress is underestimated for U_{10} <6 m s^{-1}. By not shoaling c_p, stress is underestimated for U_{10} <6 m s^{-1} and overestimated for U_{10} >6 m s^{-1}. An increase in H_{sig} increases $u_{*\mathrm{wave,sw}}$, and becomes important at $H_{sig} = 1.5$ m where it becomes large enough to modify the total u_* up to 10 m s^{-1} (Figure 10c). To summarize, H15 wave stress estimates are sensitive to H_{sig}, and shoaling both c_p and H lead to increased $u_{*\mathrm{wave,sw}}$, with the largest effects observed for U_{10} <6 m s^{-1} and h<15 m.

S09 and H15 were selected to evaluate the relevance of sea and swell contributions across the inner shelf due to their explicit description of swell wave stress being separate from wind stress, however, it is assessed that S09 does not effectively account for wave stress. S09 is an analytical model that is effective in demonstrating how vertical winds $U(z)$ are modified in the presence of waves to explain wind maximums at the surface and conditions within the WBL. Chen et al. (2019) validated S09 while accounting for shoaling in 16 m water depth, but did so by modifying the tuning coefficient C_β from a value of 32 (originally formulated by Hanley and Belcher (2008) and used by S09) to a value of 16. This adjustment effectively reduces the growth contribution (sea) by half. Over accounting for sea wave stress can also be realized through understanding the model variables itself. The contribution of sea wave stress is first accounted for via z_0, and second in the wave spectrum, effectively doubling the wave growth contribution. The S09 swell term is always negative (Figure 13d) and therefore, will never have a direct relationship with H15. The H15 response to shoaling more appropriately defines conditions observed in the field, however, only has relevance at z=10 m in a narrow band of *h* and U_{10}. H15 also does not account for wave breaking, only via H_{sig}. The maximum H_{sig} that H15 can resolve is determined (Figure 7c) whereby weighting the H_{sig} values in Figure 7c by γ_{sw} results in $H_{sig} < 2$ m (H15 limits). Figure 7c is limited to values of 80% probability of occurrence using Figure 14a, determined to be H_{sig} =4 m. The region of largest swell stress effects of *h*<15 m correspond to H_{sig} >3 m and *U*<8 m s^{-1} (Figure 7c). By using the limits of the model and the limits of what is likely to be observed in the field, the results say that H15 can only evaluate H_{sig} <4 m and U_{10} <8 m s^{-1} outside of breaking.

Next, H15 is evaluated based on the likelihood of occurrence based on the MB climatology. The discussion of the H15 formulation so far only described the important aspects of shoaling and wind speed for two wave heights. As it is difficult to show the importance of many variable simultaneously, the goal is to evaluate $u_{*\mathrm{wave,sw}}$ as functions of H_{sig}, n_p, and U_{10} that will not focus on the depth dependence. The notion is that if the

shoaled variables were H_{sig}, n_p, and U_{10}, $u_{*\mathrm{wave,sw}}$ would be defined as the following. In the H15 discussion, γ_{sw} was important as it changed as a function of depth and therefore influenced $u_{*\mathrm{wave,sw}}$. To reduce the depth variability of γ_{sw}, $\gamma_{sw,o}$ was used for simplification. The probability density of H_{sig} and n_p for MB results in H_{sig} ranging from 0.5-8 m and n_p ranging from 0.04 to 0.3 Hz (Figure 14a). Most (80% defined by the white dashed line in Figure 14a) of the H_{sig} occurs from 0.75-4 m and n_p occurs from 0.05 to 0.15 Hz. Therefore, H15 will be limited by the occurrence of H_{sig} and n_p. H15 for $u_{*\mathrm{wave,sw}}$ is evaluated for U_{10} =1-10 m s^{-1} (Figure 14cdefghijkl), as 10 m s^{-1} was found to be an upper wind speed for H15 in Figures 10b and 11b. No values are computed if the occurrence of H_{sig} and n_p does not occur in Figure 7a or if $\gamma_{sw,o}$ equals zero. $u_{*\mathrm{wave,sw}}$ increases with increasing H_{sig} and n_p and has the largest range and largest values for lower wind speeds (Figure 14cdefghijkl). Though subtle, $u_{*\mathrm{wave,sw}}$ is smaller for large winds at lower n_p and smaller H_{sig} (see darker blue region increases across Figure 14cdefghijkl in the lower left corner). The $u_{*\mathrm{wave,sw}}$ as function of H_{sig} and n_p is shown, however it does not provide the likelihood of occurrence. The $u_{*\mathrm{wave,sw}}$ in Figure 14cdefghijkl is weighted by the probability density function in Figure 14a, and the mean and standard deviation of the weighted $u_{*\mathrm{wave,sw}}$ are estimated per U_{10} (Figure 14b – black squares and vertical lines). The mean weighted $u_{*\mathrm{wave,sw}}$ is relatively constant for $U_{10} \leq 6$ m s^{-1} after which it decreases with increasing U_{10}. Similarly, the variability of weighted $u_{*\mathrm{wave,sw}}$ is constant for $U_{10} \leq 6$ m s^{-1} and then increases with increasing U_{10}. $\boldsymbol{u_{*\mathrm{wind,sea}}}$ is evaluated for context. For U_{10} <6 m s^{-1}, $u_{*\mathrm{wave,sw}}$ is relatively larger than $\boldsymbol{u_{*\mathrm{wind,sea}}}$ and is relatively equal at U_{10} =6 m s^{-1}. For U_{10} >6 m s^{-1}, $u_{*\mathrm{wave,sw}}$ is relatively smaller than $\boldsymbol{u_{*\mathrm{wind,sea}}}$. When U_{10} =10 m s^{-1}, $u_{*\mathrm{wave,sw}}$ would represent approximately 20% of $\boldsymbol{u_*}$. If γ_{sw} was used for shallow water depths, $u_{*\mathrm{wave,sw}}$ would be near zero (Figure 7b). Statistically speaking, the contribution $u_{*\mathrm{wave,sw}}$ is

significant for small winds (U_{10} <7 m s^{-1}) and represents nearly 100% to 50% of the contribution.

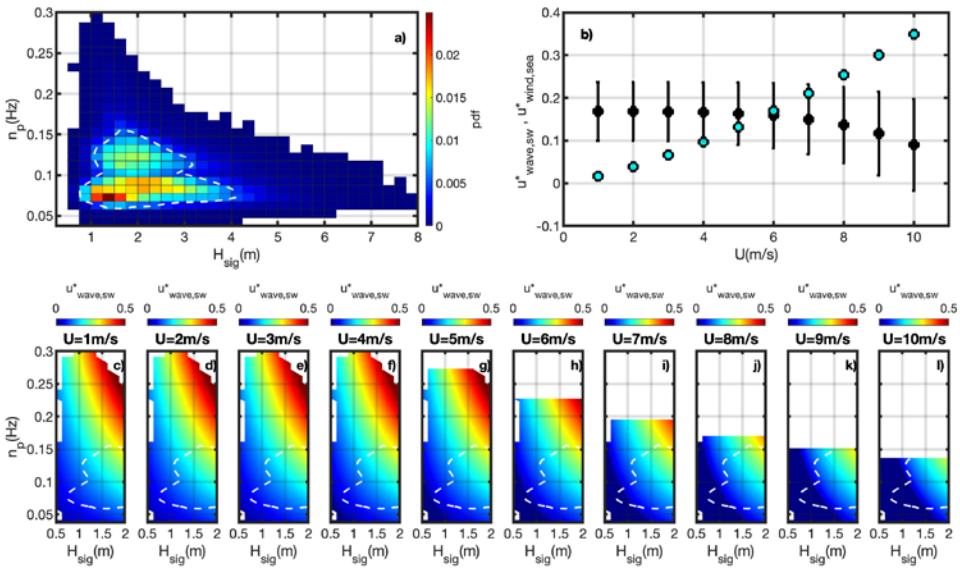

Figure 14. Probability density function of H_{sig} and wave frequency, with values of 80% probability enclosed by the white dashed line.(a). u_* of H15 wind sea (aqua circles) and swell term mean (solid black circles) and standard deviation (solid lines) weighted by (a) and evaluated at U_{10} (b). H15 $u_{*wave,sw}$ for H_{sig} =0.5-2 m vs frequency for U_{10} =1-10 m s^{-1} where the white dashed line is 80% of the data from Figure 16a (c,d,e,f,g,h,i,j,k,l).

V. CONCLUSION

C_D, τ, and u_* are consistently under-predicted in shoaling regions by models empirically parameterized by open ocean estimates. Both winds and waves contribute to stress at the surface, which is inherently linked to the wave height and wave speed. Traditional models based on a logarithmic wind profile (MOST) use average wave statistics and account for waves via aerodynamic roughness length, z_0. This is analogous to C_D in that it accounts for wave contributions via a single empirically derived parameter. Traditional approaches work in open ocean conditions for a certain range of conditions, however, fail when the balance of wave contributions are greater than or relatively similar to wind contributions. When considering the balance of wave contributions to stress across the inner shelf, wave phase velocity decreases and wave height increases with decreasing depth, suggesting that wave stress should increase. Observations across this region are sparse, and difficult to obtain due to depth limited instrumentation. The studies that have been achieved (MacMahan 2017; Ortiz-Suslow et al. 2015; Ortiz-Suslow et al. 2018) show a consistent trend of under-predicted surface stress by varying amounts (O(2) to O(4)). Only Chen et al. (2019) observed a decrease in stress in the deeper end of the shoaling region (h=16 m) that also deviated from traditional modelled values. Appropriately accounting for surface stress across the inner shelf is therefore not sufficiently achieved through bulk parameterization models. It is suggested that by more appropriately accounting for the wave stress contribution via spectral contributions and concomitant shoaling will account for the higher observed stress.

Two simple models were selected that explicitly describe swell wave stress separately from wind stress. S09 is an analytical model that spectrally describes the contribution of sea and swell wave stress vertically, originally designed for deep water, but adapted and validated by Chen et al. (2019) at h=16 m at a single location. H15 is an empirical model based on bulk statistics derived from spectral wave observations that predicts stress at 10 m only, validated in deep water, and tested broadly in a shoaling region with promising results (Ortiz-Suslow et al. 2018). Due to the lack of existing observations,

a sensitivity analysis of these models is explored to provide insight into how wave stress evolves spatially over the shoaling region. This is achieved by modifying the model input variables to incorporate depth dependence by including wave shoaling and to provide a realistic context by using MB climatology. Net wave contributions were computed spectrally for sea and swell vice using average wave statistics commonly used in z_0 models. Improvements were made on previous estimates for apportioning sea and swell that used peak frequency by applying a weight to the H_{rms} bulk statistic using n_p, which varies with depth. This is suggested to better account for the entire wave spectrum, and therefore, to improve stress estimates over the inner shelf.

The H15 model provided the most valid approach to explicitly describing the contribution of wave stress when compared with S09. S09 accounts for sea wave influences both spectrally and via z_0, effectively doubling the negative contribution to surface stress attributed to sea waves. The S09 swell term is always negative, and therefore, does not appropriately define the mechanics of how wave stress inputs evolve over the inner shelf. Chen et al. (2019) observed negative stress which validated S09, however, this only looked at one location outside of the region where the largest shoaling influences were determined to occur by this study (h<15 m). The H15 response to shoaling more appropriately defines conditions observed in the field (MacMahan 2017; Ortiz-Suslow et al. 2015; Ortiz-Suslow et al. 2018). By accounting for shoaling, swell wave stress can be up to 50% higher from an offshore depth of 30 m to an inshore depth of 5 m for winds <5 m s^{-1}. By neglecting to shoal H_{sig} (keeping H constant) stress is under-estimated for U_{10} <6 m s^{-1} for h<25 m, with the error magnitude increasing with decreasing depth. By not shoaling c_p, stress is under estimated for U_{10} <6 m s^{-1} and overestimated for U_{10} >6 m s^{-1}. H15 model predictions are also sensitive to H_{sig}. Wave stress becomes relatively more important for H_{sig} =1.5 m, becoming large enough to modify the total u_* for winds up to 10 m s^{-1}. The high sensitivity to H_{sig}, and the region of low winds where the largest effects occur, suggests a potential reason for the large variability of C_D observed in shoaling regions.

Overall, the results provided modelled spatial estimates of wave stress in the absence of satisfactory exisiting observations over the inner shelf. The importance of incorporating depth dependence and accounting for the wave spectrum revealed higher stress predictions across the shoaling region. Being able to understand and explicitly describe wave stress contribuitions would extend the range of conditions models will work, not only for shoaling regions, but also for offshore regions. Validation of these results via field observations are required to substantiate these claims, which is outside the scope of this thesis.

THIS PAGE INTENTIONALLY LEFT BLANK

LIST OF REFERENCES

Chalikov, and Babanin, 2019: Parameterization of wave boundary layer. *Atmosphere*, **10,** 686.

Chen, S., F. Qiao, W. Jiang, J. Guo, and D. Dai, 2019: Impact of surface waves on wind stress under low to moderate wind conditions. *Journal of Physical Oceanography*, **49,** 2017–2028.

Cifuentes-Lorenzen, A., J. B. Edson, and C. J. Zappa, 2018: Air–sea interaction in the southern ocean: exploring the height of the wave boundary layer at the air–sea interface. *Boundary-Layer Meteorology*, **169,** 461–482.

Dawe, J. T., and L. Thompson, 2006: Effect of ocean surface currents on wind stress, heat flux, and wind power input to the ocean. *Geophysical Research Letters*, **33**.

Dean, R. G., and R. A. Dalrymple, 1991: *Water Wave Mechanics for Engineers and Scientists.* World Scientific, 371 pp.

Donelan, M. A., F. W. Dobson, S. D. Smith, and R. J. Anderson, 1993: On the dependence of sea surface roughness on wave development. *Journal of Physical Oceanography*, **23,** 2143–2149.

Drennan, W. M., P. K. Taylor, and M. J. Yelland, 2005: Parameterizing the sea surface roughness. *Journal of Physical Oceanography*, **35,** 835–848.

Drennan, W. M., H. C. Graber, D. Hauser, and C. Quentin, 2003: On the wave age dependence of wind stress over pure wind seas. *Journal of Geophysical Research*, **108**.

Edson, J. B., A. A. Hinton, K. E. Prada, J. E. Hare, and C. W. Fairall, 1998: Direct covariance flux estimates from mobile platforms at sea. *Journal of Atmospheric and Oceanic Technology*, **15,** 547–562.

Fewings, M. R., and S. J. Lentz, 2010: Momentum balances on the inner continental shelf at Martha's Vineyard Coastal Observatory. *Journal of Geophysical Research*, **115**.

Garratt, J. R., 1977: Review of drag coefficients over oceans and continents. *Monthly Weather Review*, **105,** 915–929.

Garratt, J. R., 1992: *The Atmospheric Boundary Layer.* Press Syndicate of the University of Cambridge.

Hanley, K. E., and S. E. Belcher, 2008: Wave-driven wind jets in the marine atmospheric boundary layer, **65,** 2646–2660.

Harris, D. L., 1966: The wave-driven wind. *Journal of the Atmospheric Sciences*, **23,** 688–693.

Högström, U., E. Sahlée, A.-S. Smedman, A. Rutgersson, E. Nilsson, K. K. Kahma, and W. M. Drennan, 2015: Surface stress over the ocean in swell-dominated conditions during moderate winds. *Journal of the Atmospheric Sciences*, **72,** 4777–4795.

Jones, I. S. F., and Y. Toba, 2001: *Wind Stress Over the Ocean.* Cambridge University Press.

Kaimal, J. C., and J. J. Finnigan, 1994: *Atmospheric Boundary Layer Flows - Their Structure and Measurement* Oxford University Press, 304 pp.

Kitaigorodskii, S. A., and Y. A. Volkov, 1965: On the roughness parameter of the sea surface and the calculation of momentum flux in the near-water layer of the atmosphere. *Izvestiya, Atmospheric and Oceanic Physics*, **1,** 973–988.

Klein, P., and B. Coste, 1984: Effects of wind-stress variability on nutrient transport into the mixed layer. *Deep Sea Research Part A. Oceanographic Research Papers*, **31,** 21–37.

Large, W. G., and S. Pond, 1980: Open ocean momentum flux measurements in moderate to strong winds. *Journal of Physical Oceanography*, **11,** 324–336.

MacMahan, J., 2017: Increased aerodynamic roughness owing to surfzone foam. *Journal of Physical Oceanography*, **47,** 2115–2122.

Munk, W., and C. Wunsch, 1998: Abyssal recipes II: energetics of tidal and wind mixing. *Deep Sea Research Part I: Oceanographic Research Papers*, **45,** 1977–2010.

Ortiz-Suslow, D. G., B. K. Haus, N. J. Williams, N. J. M. Laxague, A. J. H. M. Reniers, and H. C. Graber, 2015: The spatial-temporal variability of air-sea momentum fluxes observed at a tidal inlet, **120,** 660–676.

Ortiz-Suslow, D. G., B. K. Haus, N. J. Williams, H. C. Graber, and J. H. MacMahan, 2018: Observations of air-sea momentum flux variability across the inner shelf. *Journal of Geophysical Research: Oceans*.

Reeve, D., 2018: *Coastal Engineering: Processes, Theory and Design Practice.* Third edition. ed. CRC Press.

Semedo, A., K. Sušelj, A. Rutgersson, and A. Sterl, 2011: A global view on the wind sea and swell climate and variability from ERA-40, **24,** 1461–1479.

Semedo, A., Ø. Saetra, A. Rutgersson, K. K. Kahma, and H. Pettersson, 2009: Wave-induced wind in the marine boundary layer. *Journal of the Atmospheric Sciences*, **66,** 2256–2271.

Shabani, B., P. Nielsen, and T. Baldock, 2014: Direct measurements of wind stress over the surf zone, **119,** 2949–2973.

Stull, R. B., 1988: *An Introduction to Boundary Layer Meteorology*. Kluwer Academic Publishers.

Thornton, E. B., and R. T. Guza, 1983: Transformation of wave height distribution. *Journal of Geophysical Research*, **88,** 5925.

Wyngaard, J. C., and M. A. LeMone, 1980: Behavior of the refractive index structure parameter in the entraining convective boundary layer. *Journal of the Atmospheric Sciences*, **37,** 1573–1585.

THIS PAGE INTENTIONALLY LEFT BLANK

INITIAL DISTRIBUTION LIST

1. Defense Technical Information Center
   Ft. Belvoir, Virginia

2. Dudley Knox Library
   Naval Postgraduate School
   Monterey, California